Proceedings of the 2nd Marine Energy Technology Symposium
METS2014
April 15-18, 2014, Seattle, WA

EXPERIMENTAL AND NUMERICAL ANALYSIS OF A SCALE-MODEL HORIZONTAL AXIS HYDROKINETIC TURBINE

Teymour Javaherchi*
University of Washington - NNMREC
Seattle, WA, USA

Nick Stelzenmuller
University of Washington - NNMREC
Seattle, WA, USA

Joseph Seydel
Boeing Co.
Seattle, WA, USA

Alberto Aliseda
University of Washington - NNMREC
Seattle, WA, USA

ABSTRACT

This paper presents an experimental/numerical study of a scale-model Horizontal Axis Hydrokinetic Turbine (HAHT). The model turbine is based on the DOE Reference Model 1 (DOE RM1), with a modified geometry to reproduce performance at the flume scale Reynolds numbers. These modifications were necessary to overcome the strong Reynolds number effect on the NACA$-$6 airfoil family used on the design, and therefore on the device performance in experimental analysis. The performance and wake structure of a single turbine was analyzed with measurements conducted on a 45:1 scale physical model of the modified design of the DOE RM1 rotor. The details of the rotor flow field and wake evolution are analyzed from numerical solution of the RANS equations solved around a computational model of the scale-model turbine. A comparison between the experimental and numerical results is presented. These comparisons highlight the strengths as well as limitations of the experimental and numerical analysis for these types of HAHT characterizations. On a more general sense, these comparisons provide useful guidelines for developing a set of experimental flume scale data and to use it to validate numerical tools, and as pilot projects start to go in the water in the US, to perform a similar type of analysis and design validation of full scale devices.

*Corresponding Author: teymourj@uw.edu

1 INTRODUCTION

Marine HydroKinetic (MHK) turbines require engineering methods that can provide quantitative answers to open questions regarding their performance, optimization, and environmental effects. These advanced design, evaluation and optimization methods can speed up the development process from concept to prototype to pilot demonstrator, and reduce the capital requirements of this incipient industry.

Many previous studies [1, 2, 3, 4, 5] have addressed some of these questions by either numerical simulation or laboratory experiments using a wide range of turbine geometries. The creation of the DOE Reference Model 1 (DOE RM 1) reference turbine geometry allows for direct comparison of results and analysis from different research groups in an open dialog that can benefit this community. Here, the numerical simulations and experimental results using a modified version of this reference model, operating in the same range of Tip Speed Ratios (TSR) as the original DOE RM1, to study the performance and wake hydrodynamics of this Horizontal Axis Hydrokinetic Turbine (HAHT) is presented.

Laboratory-scale testing of HAHT is used to validate numerical models and gain insight into the performance and wake dynamics of HAHT. Recirculating flumes and towing tanks are used for these tests, with measurements of the torque produced at the shaft, the rotational speed, and the drag (or thrust) force on the HAHT, as well as the flow velocity field. Multiple experimental studies in the literature [6, 7, 8] have measured a variety of turbine performance metrics and wake structure, to characterize

the performance of single HAHT with various rotor geometries. These studies typically provide insight into the fluid dynamics and energy conversion process of MHK turbines, although unfortunately through incomplete information that limits the certainty and quantitativeness of the conclusions.

The DOE Reference Model 1 (DOE RM 1) was proposed as an open source design for HAHT that could be used to benchmark computational and experimental studies. Lawson et al. [3] have performed a detailed numerical analysis on the DOE RM1 model using RANS simulation with a rotating frame turbine implementation, as well as with a sliding mesh implementation that included the two side-by-side turbines and the central support column. They investigated the effect of mesh resolution on numerical modeling results and characterized the turbine performance using both steady and transient models, showing good agreement between unsteady and steady simulations for the optimal operating conditions (TSR =6.3 and $\theta_p = 0°$), where the flow is fully attached to the turbine blade. They did find, however, that for other operating conditions, unsteady models might be the better choice in order to provide more accurate results for the flow field and turbine performance characterization in situations where the flow is separated in a significant part of the blade suction surface.

Kang et al. [4] recently reported on an LES simulation on the Gen4 KHPS turbine developed by Verdant Power for the Roosevelt Island Tidal Energy (RITE) project in the East River in New York. They investigated flow field behavior in the near wake of this turbine, the grid resolution effect on the numerical results and the coherent vortex structures shed into the turbine's near wake. Kang et al. concluded that the pressure field near the turbine blades is not significantly affected by the structural support of the turbine (i.e. pylon, nacelle, etc.) and interpreted this observation as suggesting that the simulation of the isolated rotor can be used as a valid approximation for predicting the power of a single HAHT. Kang et al. used the limited field data available to validate their numerical model and propose that their validated numerical tool can be used to investigate site specific variations such as complex bathymetry and sheared velocity profile at the field site on the performance of turbines.

This paper investigates different aspects of HAHTs via comparison between experimental and numerical results. Similar to the studies cited above, we compare efficiency and flow field in the wake of a single HAHT. Unlike existing studies, we compare flume experiments and computational results under the exact same conditions and scale (Reynolds number). Our goal is to develop a general methodology to investigate the performance and the fluid dynamics around and in the wake of the HAHT rotors, and to create a database of experimental results that can be used to validate engineering design and analysis tools.

Section 2 presents description of the experimental setup used for performance studies and flow field analysis in the wake of the modified scaled model of the DOE RM1 turbine, and discussion on the experimental measurements. Section 3, discusses numerical techniques for implementation of MHK turbines in RANS simulations for characterization of turbine efficiency and flow field. Section 4 compares experimental measurements against computational results at matched Reynolds numbers ($Re = 7.8\ 10^4 - 1.4\ 10^5$) and channel confinement and turbulence intensities, under a wide range of Tip Speed Ratios ($TSR = 5.5 - 10.33$). Finally, Section 5 briefly describes applicability and limitations of the numerical models for performance and flow field characterization of full-scale turbines.

2 Experimental Analysis

2.1 Rotor and nacelle design

Preliminary experimental results obtained from laboratory testing of a 45:1 geometrically-scaled DOE RM1 rotor showed a low coefficient of performance ($C_p^{maximum} \approx 20\%$) compared to predictions of full-scale DOE RM1 performance based on Blade-Element-Momentum Theory ($C_p^{maximum} \approx 45\%$). These results are shown in figure 1.

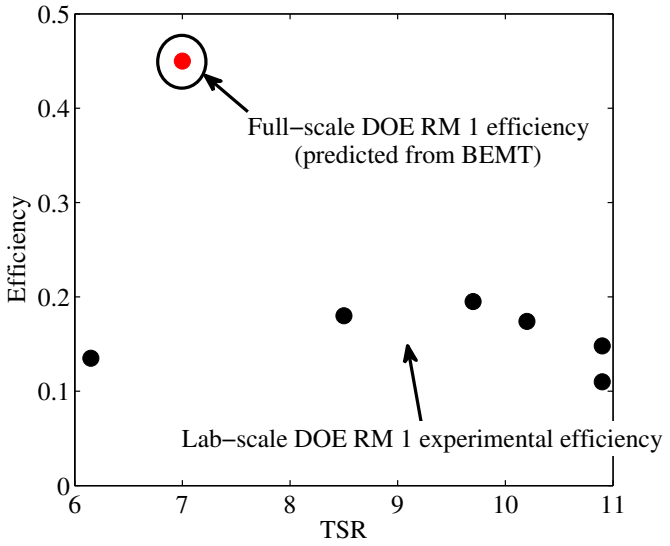

FIGURE 1. COMPARISON BETWEEN THE EXPERIMENTAL VALUE OF EFFICIENCY FOR THE DOE RM1 LAB. SCALED MODEL AND NUMERICAL VALUE OF EFFICIENCY FOR THE FULL-SCALE DOE RM1 MODEL USING BLADE-ELEMENT-MOMENTUM THEORY.

The relatively low efficiency of the geometrically-scaled DOE RM1 turbine compared to numerically predicted efficiency suggests that the laboratory-scale rotor should be modified in order to be dynamically similar to the full-scale DOE RM1 rotor.

The rotor was redesigned to match the efficiency and peak performance tip speed ratio of the full-scale DOE RM1.

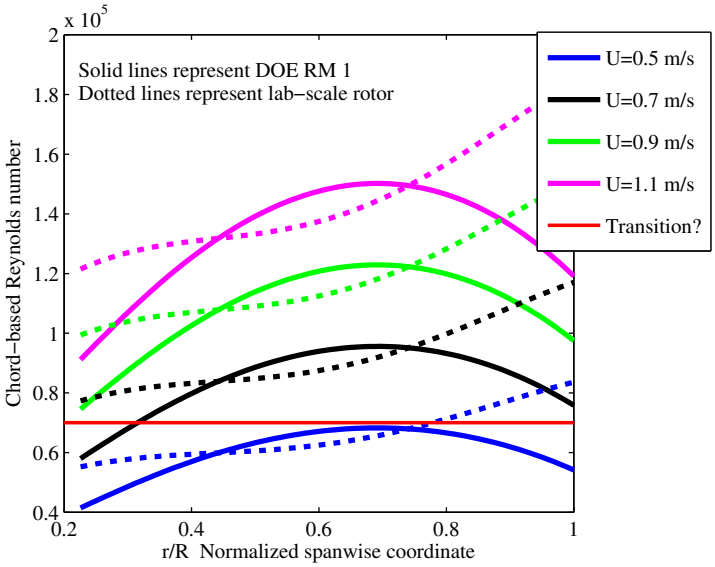

FIGURE 2. LOCAL REYNOLDS NUMBER ($\frac{U_R C}{NU}$, WHERE C IS THE CHORD LENGTH, U_R IS THE RELATIVE VELOCITY, AND ν IS THE KINEMATIC VISCOSITY) ALONG THE SPAN OF THE BLADE, PLOTTED FOR THE GEOMETRICALLY-SCALED DOE RM1 AND THE MODIFIED LABORATORY-SCALE ROTOR FOR VARIOUS FREESTREAM VELOCITIES AT TSR=7.

The relatively poor performance of the geometrically-scaled rotor was determined to be a Reynolds number effect; specifically, associated to the sharp decrease in foil performance at some critical Reynolds number due to laminar separation bubble dynamics described by Lissaman [9]. The redesigned rotor maximizes the local Reynolds number along the blade, within the constraints of matching the optimum TSR of the full-scale rotor and the maximum rotor diameter that could be tested in the flume at a reasonable blockage ratio. Figure 2 shows the local Reynolds number along the blade at several free-stream flow speeds for the geometrically-scaled DOE RM1 and the modified rotor. The foil section used in the DOE RM1 is the NACA 63-424 foil, for which the critical Reynolds number is estimated to be at 10^5; the foil used in the redesigned rotor was the NACA 4415 foil, chosen as a compromise between structural integrity and experimentally demonstrated performance at low Reynolds numbers (the critical Reynolds number for this airfoil has been *measured* at 7 10^4). The open source design code HARP−Opt [10] was used with NACA 4415 experimental wind tunnel data to optimize chord and twist distributions. Details of the modified laboratory-scale rotor design, nacelle design, instrumentation, and testing procedure are given by Stelzenmuller [11].

The modified 45:1 scale model consists of a 0.45 m diameter turbine rotor manufactured on a CNC mill from aluminum and a 0.1 x 1 m cylindrical nacelle. The nacelle contains a torque sensor (TFF325 Futek, Irvine, California), magnetic encoder (RM22 RLS, Komenda, Slovenia), and a magnetic particle brake (Placid Industries, Lake Placid, NY) used to apply shaft loading. The torque sensor and magnetic encoder are wired to an analog-digital converter and acquisition system (PCIe-6341 National Instruments, Austin, Texas) sampled at 1000 Hz. The turbine model is mounted to a vertical post extending from the top of the flume to the nacelle. The turbine CAD model is shown in Figure 3.

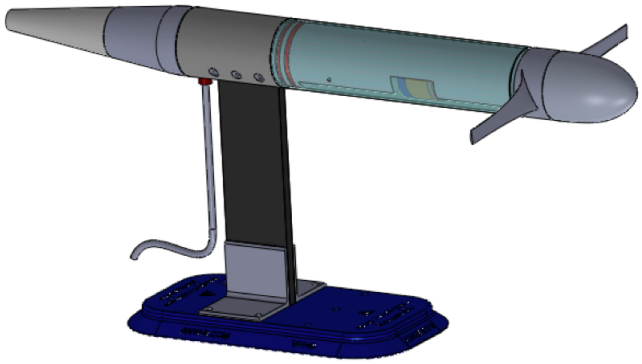

FIGURE 3. CAD MODEL OF THE MODIFIED SCALED HAHT FORM THE DOE RM 1 GEOMETRY, BUILT FOR EXPERIMENTAL AND NUMERICAL ANALYSIS.

2.2 Laboratory Setup

Flume testing on a modified version of the DOE Reference Model 1 (DOE RM 1) geometry was carried out at the Bamfield Marine Science Center, with a 1 m wide by 0.8 m depth cross section and 12.3 m long test section. The blockage ratio was 20%. ADV (Vector Nortek, Oslo, Norway) and PIV (LaVision Gmbh., Goettingen, Germany) systems were used to characterize the flow upstream and in the wake of the turbine within the predefined interrogation windows, aligned parallel to the flow and on the axis of rotation of the turbine, as shown in figure 4. PIV data was taken for 40 seconds at 5 Hz for each imaging location and the results processed under the assumption of statistically steady free-stream flow.

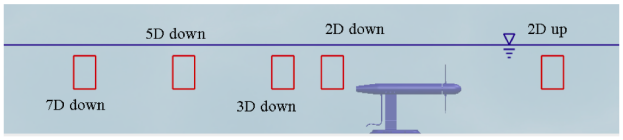

FIGURE 4. PIV IMAGING WINDOWS FOR MEASUREMENT OF VELOCITY UP- AND DOWNSTREAM OF THE TURBINE DURING THE EXPERIMENT.

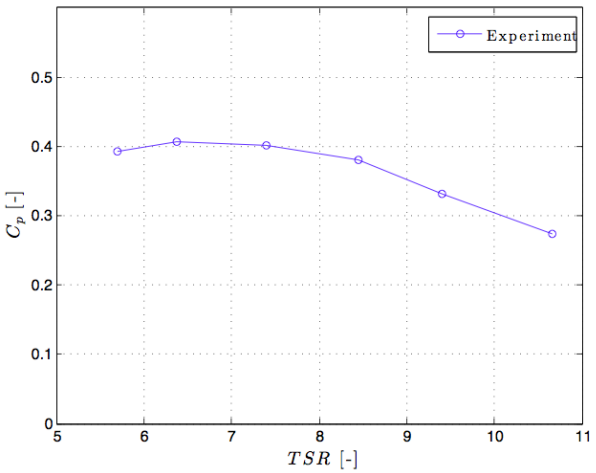

FIGURE 5. PERFORMANCE CURVE (C_P VS. TSR) DEVELOPED FROM THE EXPERIMENTAL ANALYSIS OF A SINGLE SCALED MODEL HAHT.

2.3 Experimental Results

2.3.1 Performance Curve (C_p vs. TSR) Figure 5 shows the variation of the turbine efficiency as a function of Tip Speed Ratio (TSR). The measured torque and rotational velocity of the turbine were time-averaged and multiplied to calculate the power extracted by the turbine. The efficiency was normalized using the kinetic energy flux measured from PIV at a position 2 diameters upstream of the turbine. It can be seen in figure 5 that, as the value of the TSR increases, the efficiency of the turbine decreases. Under this condition the angle of attack for the majority of the airfoils along the blade span are below their optimum and the power extracted by the turbine decreases as a result.

An interesting observation from figure 5 is that the measured efficiency does not have a clearly defined maximum. In other words, the turbine efficiency is almost constant for a wide range of TSR values, decreasing from the theoretical peak around 7 to about 5.5 with little change in performance. This is in contradiction with aero- and hydrodynamic principles: decrease in TSR will result in the increase of AOA along the blade root. Large AOA values result in flow separation and unsteadiness along the blade span, and eventually stall, especially close to the root of the blade. These phenomena will decrease the efficiency of the turbine. Further analysis of the experimental data showed that as the turbine operates under lower TSRs conditions, there is an increase in fluctuations of the rotational velocity, that affects the flow structure at the blade surface, and therefore rotor performance. Figure 6 shows the temporal variation of turbine's rotational velocity at two ends of the TSR range explored (TSR=5 and 10). The green and blue curves show the temporal variation of rotational speed normalized with the mean for TSRs equal to 5 and 10, respectively. Figure 6 confirms that at TSR=10, the rotational speed have very small fluctuations. At lower TSR, however, the fluctuations are relatively large and there are even a few large excursions (beyond 3 times the signal rms) during the 60 seconds of measurements. Our hypothesis is that these large fluctuations in the rotational velocity postpone the potential stall phenomenon at low TSR values (high AOA values). Therefore, the efficiency of turbine remains high as the TSR value decreases and turbine still performs close to its maximum efficiency. To visualize the effects of the angular velocity fluctuations in the flow field on the rotor blade surfaces, we will need to explore the blade-resolved RANS simulations.

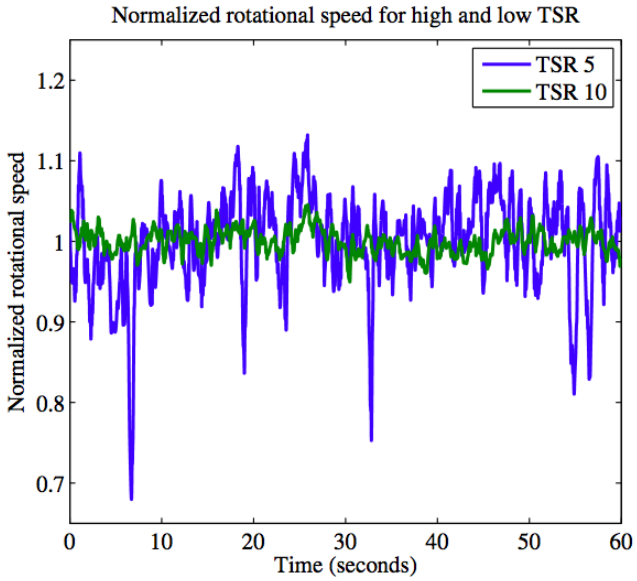

FIGURE 6. TEMPORAL VARIATION OF MEASURED NORMALIZED ROTATIONAL SPEED OF TURBINE DURING TWO EXTREME END OF TSR RANGE (TSR=5 AND 10).

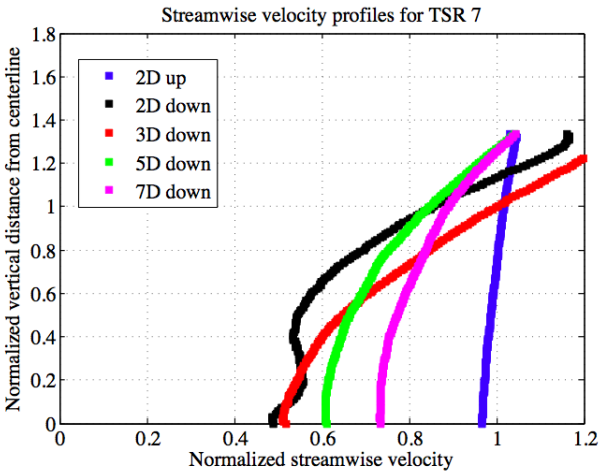

FIGURE 7. MEASURED STREAMWISE VELOCITY, AVERAGED OVER TIME AND ALONG THE STREAMWISE COORDINATE INSIDE THE PIV DOMAIN, AT VARIOUS DISTANCES UP- AND DOWNSTREAM OF A SINGLE TURBINE AT TSR=7.

2.3.2 Wake Recovery The velocity fields 2 diameters upstream of the turbine and at various distances downstream of the turbine were measured from PIV at vertical-streamwise planes that covered the flow from the centerline to very near the free surface (the position of the imaging windows is shown in schematic form in figure 4). These measurements were averaged over the interval of acquisition (60 *s*) and along the streamwise coordinate inside each PIV domain, that is for all the measurement points that are at the same distance from the turbine axis of rotation (and the same depth, since the PIV plane is vertical). The averaged velocity measurements are presented in figure 7.

Each curve represents the value of the streamwise velocity at one position with respect to the turbine rotor (2D upstream, and 2D, 3D, 5D, and 7D downstream) normalized by the free-stream velocity at the inlet of the flume. The blue curve shows the velocity profile 2D upstream the turbine. There is a slight deceleration region from the centerline to the tip of the blade, which is due to the blocking effect of the turbine rotor. Near the top of the flume, there is a slight acceleration due to the flume confinement and rotor blockage effect. Overall, the variations in the velocity profile 2D upstream the turbine are very small. The black curve shows the velocity profile 2D downstream of the turbine. The velocity deficit is maximum at this station, which falls right at the back end of the turbine nacelle. In this velocity profile, there exists a bulge of rapid deceleration of the flow, which is due to the effect of the nacelle and its tapered tailcone, as shown in figure 3. Moving further downstream, this bulge smoothes out, the velocity deficit becomes weaker and wake recovery is observed. The green curve shows that at the 5D downstream station, the velocity deficit has recovered to about 60%-80% of the velocity at the turbine rotor. At the last measurement station, 7D downstream of the turbine, the velocity has recovered almost completely to about 75%-100% of the free-stream, from the rotor centerline to the blade tip near the flume free surface.

3 Numerical Analysis

3.1 Numerical Setup

In the numerical modeling part of this study, the Rotating Reference Frame (RRF) and the Blade Element Model (BEM) methodologies are used to simulate the flow field associated with the laboratory-scale model turbine. The RRF and BEM formulations are combined with the RANS equations and a turbulent closure model to investigate the effect of the Tip Speed Ratio variation (TSR=5.5 to 10.3) on the performance and wake structure of a single turbine. In this section, the theory behind each numerical model is briefly explained. Then, the numerical results from each model is presented and compared against each other.

3.1.1 Rotating Reference Frame (RRF) Model

The RRF model renders the unsteady problem of flow around a turbine blade in a fixed reference frame into a steady problem of flow with respect to the rotating reference frame moving with the blade. In this formulation, the effect of rotation is input into the equations of fluid motion by adding body forces that represent the inertial effects associated with the centrifugal and Coriolis accelerations [12]. This allows the equations to be integrated using a stationary grid and to avoid the complexity and stiffness associated with rotating mesh simulations. The trade-off in using this model is that it requires an axisymmetric domain and periodic boundary conditions.

Figure 8 shows the computational domain and boundary conditions for the RRF model. Taking advantage of the modified DOE RM 1 turbine symmetry (two bladed rotor), only half of the domain is modeled in this work. The boundary condition is constant velocity at the inlet and uniform pressure at the outlet. Cyclic-periodic boundaries are prescribed on the symmetry plane of the domain to simulate the blade rotation. The domain's top cylindrical boundary sets the limit of the computational domain. The distance between this boundary and tip of the turbine blade is about 0.275 m to match the experimental blockage ratio of 20%. This boundary is modeled with a slip-free boundary condition. Figure 8 shows the span of the blade and the geometry of the nacelle, included in the computational domain. Including the actual geometry of the blade in this model provides the opportunity to capture the details of the flow field in the near wake region.

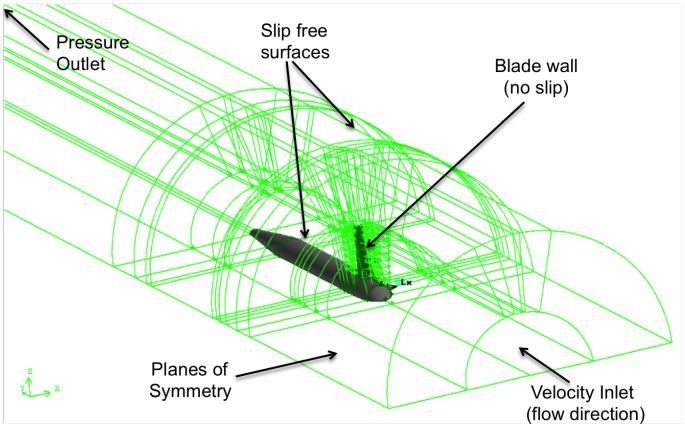

FIGURE 8. COMPUTATIONAL DOMAIN AND BOUNDARY CONDITIONS USED WITH THE RRF MODEL. THE ACTUAL GEOMETRY OF THE SCALED HAHT BLADE (GRAY REGION) IS INCLUDED IN THIS COMPUTATIONAL DOMAIN.

The RRF computational domain has approximately $4.7\text{x}10^6$ mesh elements. The mesh is structured in most of the RRF's computational domain, except for a region at the inlet, in front of the nacelle's curved head, and in the wake of the turbine, right in behind the tapered section of the nacelle. In these sections, unstructured tetrahedral elements were used to mesh the domain. The required mesh resolution around the airfoil sections and along the span of the turbine blade and other parts of the computational domain were based on the guidelines and results of previous grid resolution studies [13] and [14]. The concentration of mesh elements in the RRF domain is focused around the blade span to ensure capturing the turbulent boundary layer on the blade surfaces. The number of nodes around the airfoil sections of the blade is 152 with equal spacing. The number of nodes along the blade span is 94 and they are equally spaced. In the radial directions of the C−mesh 19 nodes were considered with the first length of 0.5 mm from blade wall. This value of first length was calculated according to the chord-based Reynolds number and the guidelines provided in [14]. For a Reynolds number of 10^5, the first length of 0.5 mm satisfies the range of Y^+ between 30-300 to capture the turbulent boundary layer along the blade span using the wall function approach. It should be noted that this mesh resolution should be modified for the full scale simulation as the Reynolds number changes by an order of magnitude.

3.1.2 Blade Element Model (BEM) The Blade Element Model (BEM) simulates the effect of the rotating blades on the fluid through a body force in the 3D space, which acts inside a disk of fluid with an area equal to the swept area of the turbine. Figure 9 shows the computational domain of the BEM and the above-mentioned disk of fluid to model the effect of the turbine, highlighted with a gray color. The boundary conditions are uniform streamwise velocity at the inlet and uniform pressure at the outlet. The outer walls of the domain are modeled as slip-free walls. The actual geometry of the nacelle is reproduced and it is modeled with a no-slip condition to capture its effect on wake recovery. In BEM, the actual geometry of the experimental domain is modeled as there is no requirement of an axisymmetric domain.

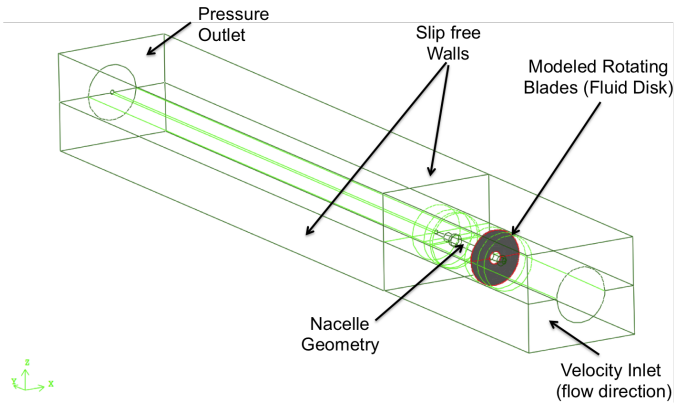

FIGURE 9. COMPUTATIONAL DOMAIN AND BOUNDARY CONDITIONS USED WITH THE BEM. THE EFFECT OF THE TURBINE IS MODELED VIA A DISK OF FLUIDWITH AN AREA EQUAL TO THE SWEPT AREA OF THE TURBINE (gray region).

In BEM, the blade is divided into thin sections from root to tip. The lift and drag forces on each section are computed from known hydrodynamic coefficients based on the angle of attack, chord length, and airfoil type. The free-stream velocity at the inlet boundary is used as an initial value to calculate the local angle of attack (AOA), and Reynolds number for each segment along the blade. Then, based on the calculated values of AOA, lift and drag coefficients are interpolated from a look-up table, which contains values of these variables as a function of AOA, Re. In this study, the look-up table of lift and drag coefficients as a function of AOA are calculated from the RRF model. The lift and drag forces are then averaged over a full turbine revolution to calculate the source term at each cell in the numerical discretization. The flow is updated with these forces and the process is repeated until a converged solution is attained.

According to previous studies [13] the BEM model is much less sensitive to mesh resolution compared to the RRF model. The reason is the simplification that BEM uses to simulate the presence of the turbine rotor. As discussed earlier, the required mesh resolution for the BEM computational domain in this study is based on the results in [13]. The BEM domain has about 5 10^5

mesh elements. Similar to the RRF domain, the BEM mesh is structured in most of the computational domain except for regions at the inlet, nacelle, and wake. In order to capture the turbulent boundary layer along the nacelle, the mesh resolution was adapted to satisfy the model requirements on the range of Y^+ of the first node near the wall.

3.2 Numerical Results

3.2.1 Performance Curve (C_p vs. TSR) Figure 12 shows the performance predicted by the RRF and BEM, relative to the experimental results. The turbine performance values at different TSR from the two models are consistent with each other, within 2-6%. For the majority of the TSR values, other than two extreme ends, BEM predicts higher performance than RRF. The root of this difference goes back to the simplifications used in modeling the hydrodynamic effect of the rotor within the BEM. The BEM averages the hydrodynamic forces on each blade segment over a cycle of rotation, thus, it is limited in capturing three dimensional flow at the blade tip or root. As shown in figure 12, both models predict a clear peak in efficiency for the scaled model turbine at TSR=8.17. Moving from this peak toward the lower TSR values, the predicted performance decreases due to increases in AOA. Higher TSRs show the agreement between RRF and BEM deteriorating. The cause of disagreement at very high TSR (i.e. TSR=10.33) is that the value of the AOA along the blade span becomes low and the three dimensionality near the blade tip becomes more dominant in the overall performance. BEM cannot accurately calculate the lift and drag forces in this small region and therefore the performance of these blade sections accurately.

3.2.2 Wake Recovery The top and bottom plots shown in figure 10 represent the streamwise velocity contours normalized with the free stream velocity on a plane parallel to the flow direction, from left to right. As shown in these two velocity contours, flow decelerates as it approaches the turbine blades and the beginning of the turbine's nacelle (white region). The turbine extracts power from the incoming flow and generates a turbulent wake. Comparison between the RRF and BEM results reveals the similarities and differences between these two numerical approaches. The top plot in figure 10 shows that the RRF captures the inhomogeneous flow field in the near wake region of the turbine ($\frac{y}{r} < 2D$) accurately. This inhomogeneity is apparent as two cyan blobs of decelerated flow near the blade tip and near the blade root. Furthermore, close to the blade tip, the shed vortices are captured via RRF in form of discrete set dark red circles. The bottom plot shows that BEM does not capture the details of the near wake region of the blade. The reason behind this limitation is that the BEM averages the hydrodynamic effect of the blade on the flow. As a result of this averaging, the inhomogeneity of the flow is smoothed out in this model. The deceleration region appears as a uniform region that starts as cyan close to the blade root and transitions to green toward the blade tip. The same process of azymuthal averaging of the hydrodynamic forces on the blade, the tip vortices are not captured by the BEM approach.

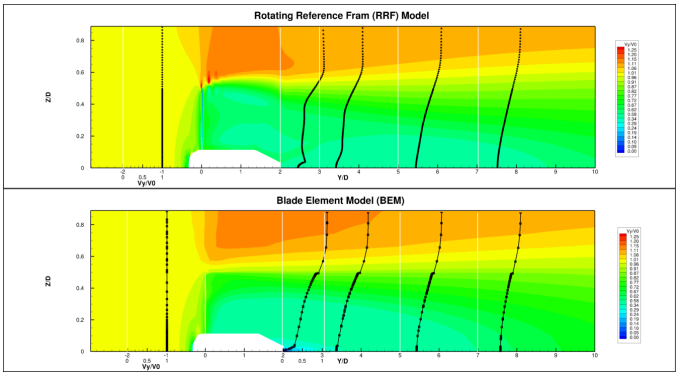

FIGURE 10. STREAMWISE VELOCITY CONTOURS, NORMALIZED WITH THE FREE STREAM VELOCITY, ON A PLANE PARALLEL TO THE FREE STREAM DIRECTION. RRF (TOP) AND BEM (BOTTOM) COMPUTATIONAL DOMAINS FOR A SINGLE TURBINE AT TSR 7. FLOW IS FROM LEFT TO RIGHT.

Despite the above-mentioned differences, the far wake is consistent when modeled via the RRF and BEM approaches. The similarities in contours shape and magnitude, visualized in figure 10 confirm this. For further quantitative comparison, figure 11 shows the velocity deficit profiles at different stations downstream of the rotor, simulated via RRF (blue) and BEM (red). The velocity deficit predictions at 2D downstream are different over the majority of the blade span, with agreement starting close to the blade tip ($0.8 < \frac{z}{r} < 1$). It should be noted that this station is located exactly downstream of the tapered end of the nacelle, and the different treatment of this region in the computations affects the shape of the velocity deficit profiles near it. More details about the simulated flow field close to the end of nacelle compared to experimental data are presented in 4.2.

At 3D downstream, the velocity deficit profiles become closer. The influence of the nacelle and the separated region behind the blunt end loses importance in the overall wake and the velocity profiles ($0.6 < \frac{z}{r} < 1$) collapse on top of each other. Stations 5D and 7D downstream present good agreement between simulated velocity deficit profiles. The flow field and velocity deficit comparison between RRF and BEM in the far wake region

of the turbine ($\frac{y}{r} > 3D$) showed in figures 10 and 11 confirms that although BEM is limited in capturing the details of the flow field in the near wake region, it is capable of simulating the far wake region as accurately as RRF, with an order of magnitude lower numerical cost (in CPU time, memory needs and human operator time in creating the mesh of the domain).

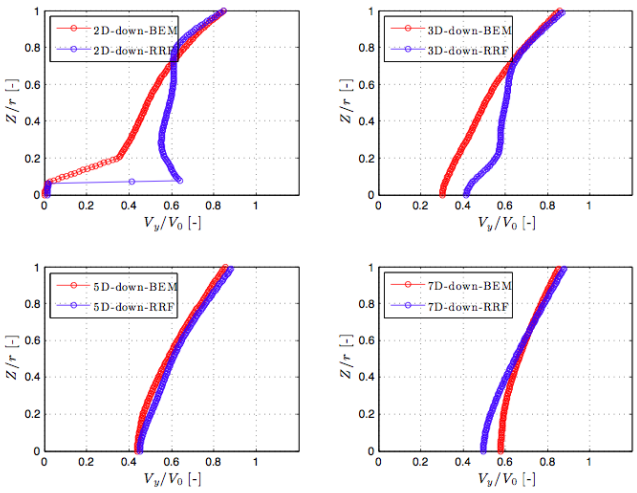

FIGURE 11. COMPARISON BETWEEN THE VELOCITY DEFICIT PROFILES SIMULATED VIA RRF (BLUE) AND BEM (RED) AT DIFFERENT STATIONS DOWNSTREAM OF THE TURBINE.

4 Comparison between Experimental and Numerical Results

4.1 Efficiency Comparison

Figure 12 presents a comparison between the experimental and numerical results for turbine performance. For the range of TSR from 8.15-10.33, the experimental and numerical performance coefficients are in very good agreement, except for the large drop in the BEM prediction at TSR of 10.33 explained earlier. The discrepancy in the efficiency between experiments and computations at lower TSR, from 5-7, brings about interesting dynamics of the turbine rotor. As discussed earlier in 2.3.1, the coefficients of performance measured at low TSR are almost constant. This is hypothesized to be due to the fluctuations in rotational velocity during the experiment. These fluctuations would result in delaying stall along the blade span, especially at the root. In the numerical computations, however, the rotational speed is imposed as a constant parameter and therefore no "dynamic" stall effect can be simulated. This lack of dynamical effects in

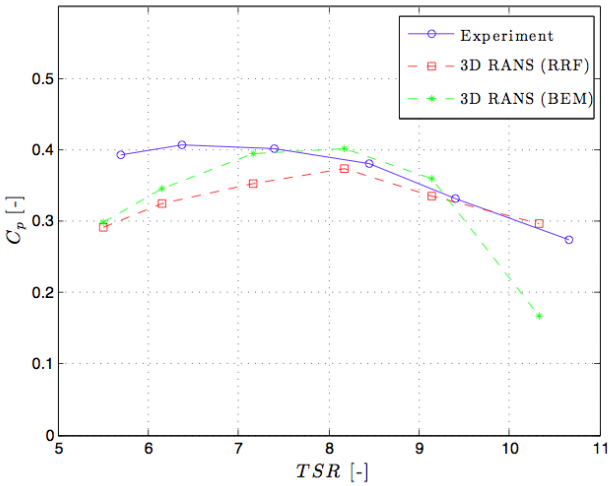

FIGURE 12. COMPARISON BETWEEN THE PERFORMANCE CURVES (C_P VS. TSR) FOR EXPERIMENTAL MEASUREMENTS AND NUMERICAL ANALYSIS (RRF AND BEM) FOR A SINGLE SCALE MODEL HAHT.

the simulation would predict a much steeper drop in performance that actually measured in the physical system, specially at low TSRs when the AOA is large across the blade span, but specially at the root. To investigate this hypothesis, the flow field along the suction side of the blade span in the RRF simulation is shown in figure 13. Wall Shear Stress (WSS) values normalized with their maxima are used to highlight regions of flow detachment. Limited streamlines are superimposed on the WSS color contours to further delineate the extent of flow recirculation. As TSR decreases, from bottom right to top left of the figure, the dark blue region of low WSS grows at the root of the blade. In this region of low WSS, the flow starts to detach from the blade span and the limited streamlines diverge from each other. Significant separated flow exists from TSR 5-7, and not from 7-10. This view supports the hypothesis that fluctuations in angular velocity in the experiment could account for the different, by postponing stall and helping to maintain a quasi-constant coefficient of performance for the turbine that is not predicted by theory or numerical simulations.

4.2 Wake Recovery Comparison

To compare the trend of wake recovery measured in the experiment and simulated via numerical models (RRF and BEM), the velocity deficit and momentum deficit at different stations downstream of the turbine are plotted superimposed in figures 14 and 15.

At 2D downstream, the profiles of velocity deficit from ex-

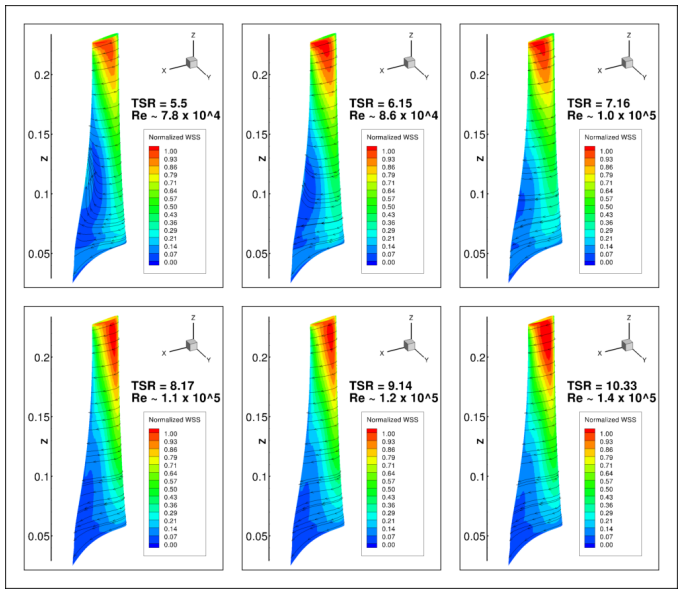

FIGURE 13. WALL SHEAR STRESS CONTOURS ALONG THE BLADE SPAN SUPERIMPOSED BY THE LIMITED STREAMLINES (SOLID ARROWS) FOR VARIOUS TSR AND CHORD-BASED REYNOLDS NUMBER.

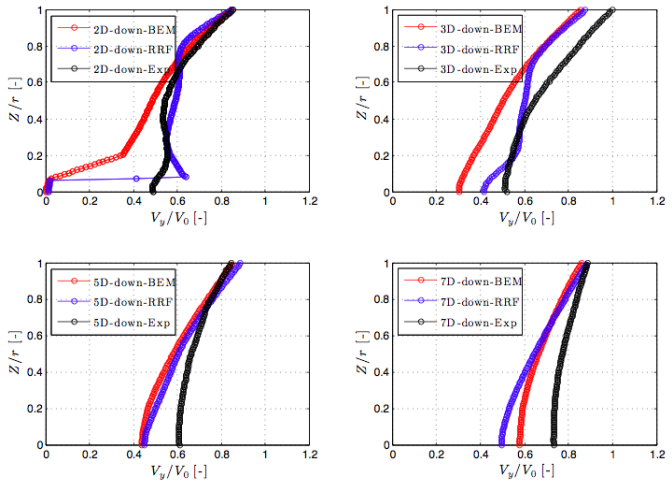

FIGURE 14. COMPARISON BETWEEN THE MEASURED (BLACK) AND SIMULATED (BLUE AND RED) VARIATION OF THE STREAMWISE VELOCITY, AT VARIOUS DISTANCES DOWNSTREAM OF A SINGLE TURBINE AT TSR=7.

periment (black) and RFF (blue) are in a fairly good agreement with each other. This is consistent with the comparison of measured vs predicted turbine coefficient of performance at $TSR = 7$, shown previously. Furthermore, this agreement confirms the ca-

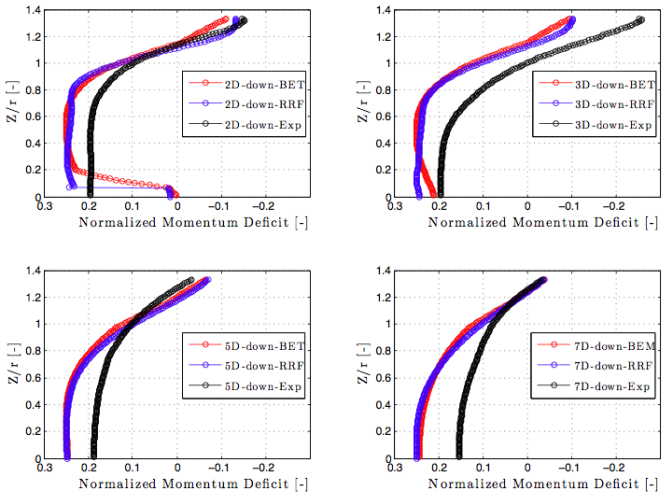

FIGURE 15. COMPARISON OF MEASURED AND PREDICTED VARIATION OF THE MOMENTUM DEFICIT AT VARIOUS DISTANCES DOWNSTREAM, FOR A SINGLE TURBINE AT TSR=7.

pability of the RRF model to capture the details of the flow field in turbine near wake region. The velocity deficit predicted by BEM (red) shows good agreement with the experimental data close to the blade tip ($0.6 < \frac{z}{r} < 1$). However, in the region close to the blade root, this agreement become poor and BEM overpredicts the deficit in the velocity. Moving further downstream, the overall shape of the experimental and numerical velocity deficit profiles are similar, but the experimental velocity deficit recovers faster than the corresponding simulated velocity deficits. We hypothesize that, in the experiment, the presence of the nacelle enhances turbulent mixing in the wake. It should be noted that in the RRF model is limited to take the nacelle wall as a a free-slip surface and the turbulent boundary layer and its effect on the turbulent mixing process in the wake of the turbine are not well captured. The BEM is not limited in modeling the nacelle, hence, the effect on the nacelle in the mixing process in the near and far wake region of the turbine could be captured more accurately. However, despite the fact that in BEM the flow over the nacelle is represented more accurately, since the flow in the effect of the rotor is averaged and the velocity deficit at the lower region of the blade is overpredicted, the trend of the wake recovery in the near wake is in not in good agreement with the experimental results.

Momentum deficit, normalized by the free-stream momentum flux is shown in figure 15 to quantify the net drag on the flow presented by the turbine rotor, and the complementary remaining momentum in the wake. Figure 15 compares the momentum deficit profiles integrated over the swept area of each blade section, at different stations downstream the turbine. The momentum deficit simulated via RRF (blue) and BEM (red) overpredict

the momentum deficit at all stations downstream of the turbine compare to the experiment. The general trends of the normalized momentum deficit for experimental and numerical results are similar to each other. The relative error in the simulations is placed in context with this more dynamically and energetically meaningful metric, as the discrepancy between experiments and simulations is of the order of 10% of the incoming momentum flux, compared to 20-30% error when computed based on the velocity deficit.

5 Summary and Conclusions

A database has been developed from the experimental analysis for a scale-model HAHT, based on the DOE RM 1 design and operating in the same range of TSR. This experimental data improves our understanding of the performance and experimental issues in scale models for marine renewable energy. It also serves as a source for validation of numerical models.

Numerical simulations were performed at the specific conditions of the experimental campaign and compared with the measurements. The RRF model was showed to be capable of capturing the details of the three-dimensional flow field in the near wake of the scale-model turbine. This model showed shed tip vortices and inhomogeneous flow behind the blade. The agreement between RRF and experimental results, coefficient of performance and velocity deficit at 2D downstream, confirmed this observation. However, the RRF showed limitations to model the effect of nacelle and its contribution to wake recovery. The BEM predicted well the coefficient of performance of the modeled turbine operating under different TSR. BEM showed limitations to model the turbine performance accurately at very low and high TSRs, underpredicting the performance of the device. However, the BEM showed promising results in simulating of the far wake region of the turbine. BEM could be a promising model for investigation of array optimization of HAHT farm spacing or potential environmental effects that depend strongly on the turbine's far wake (i.e. effect of the turbine on the sedimentation of suspended particles in a tidal channel).

REFERENCES

[1] Batten, W., Chaplin, J., Bahaj, A., and A., M., 2007. "Experimentally validated numerical method for hydrodynamic design of horizontal axis tidal turbines.". *Ocean Engineering,* ***34***, p. 1013.

[2] Batten, W., Chaplin, J., Bahaj, A., and A., M., 2008. "The prediction of the hydrodynamic performance of marine current turbines.". *Renewable energy,* ***33***, p. 1085.

[3] Lawson, M., Li, Y., and Sale, D., 2011. "Development and verification of a computational fluid dynamics model of a horizontal-axis tidal current turbine". In Proceedings of the 30th International Conference on Ocean, Offshore, and Arctic Engineering.

[4] Seokkoo Kang, S., Borazjani, I., Colby, J. A., and Sotiropoulos, F., 2012. "Numerical simulation of 3d flow past a real-life marine hydrokinetic turbine". *Advances in Water Resources*.

[5] Mycek, P., Gaurier., B., Pinon, G., and Rivoalen, E., 2011. "Numerical and experimental study of the interaction between two marine current turbines". In Proceedings of the 9th European Wave and Tidal Energy Conference.

[6] Bahaj, A., Molland, A., Chaplin, J., and Batten, W., 2007. "Power and thrust measurements of marine current turbines under various hydrodynamic flow conditions in a cavitation tunnel and a towing tank". *Renewable Energy,* ***32***(3), pp. 407 – 426.

[7] O'Doherty, T., Mason-Jones, A., ODoherty, D., Byrne, C., Owen, I., and Wang, Y., 2009. "Experimental and computational analysis of a model horizontal axis tidal turbine". In 8th European Wave and Tidal Energy Conference (EWTEC), Uppsala, Sweden.

[8] Maganga, F., Germain, G., King, J., Pinon, G., and Rivoalen, E., 2010. "Experimental characterisation of flow effects on marine current turbine behaviour and on its wake properties". *Renewable Power Generation, IET,* ***4***(6), pp. 498–509.

[9] Lissaman, P., 1983. "Low-reynolds-number airfoils". *Annual Review of Fluid Mechanics,* ***15***, pp. 223–239.

[10] Sale, D. Harp_opt user's guide. Tech. rep., National Renewable Energy Laboratory.

[11] Stelzenmuller, N., 2013. "Marine hydrokinetic turbine array performance and wake characteristics". Master's thesis, University of Washington.

[12] Warsi, Z., 1993. *Fluid Dynamics, Theoretical and Computational Approaches.* CRC Press.

[13] Javaherchi, T., and Aliseda, A., 2014. "Hierarchical methodology for the numerical simulation of the flow field around and in the wake of horizontal axis wind turbines: Rotating reference frame, blade element method and actuator disk model.". *Wind Engineering,* ***38***(2), pp. 61–82.

[14] Javaherchi, T., 2010. "Numerical modeling of tidal turbines: Methodology development and potential physical environmental effects". Master's thesis, University of Washington.